YdbH and YnbE form an intermembrane bridge to maintain lipid homeostasis in the outer membrane of *Escherichia coli*

Sujeet Kumar[a] (ID), Rebecca M. Davis[a], and Natividad Ruiz[a,1] (ID)

The outer membrane (OM) of didermic gram-negative bacteria is essential for growth, maintenance of cellular integrity, and innate resistance to many antimicrobials. Its asymmetric lipid distribution, with phospholipids in the inner leaflet and lipopolysaccharides (LPS) in the outer leaflet, is required for these functions. Lpt proteins form a transenvelope bridge that transports newly synthesized LPS from the inner membrane (IM) to OM, but how the bulk of phospholipids are transported between these membranes is poorly understood. Recently, three members of the AsmA-like protein family, TamB, YhdP, and YdbH, were shown to be functionally redundant and were proposed to transport phospholipids between IM and OM in *Escherichia coli*. These proteins belong to the repeating β-groove superfamily, which includes eukaryotic lipid-transfer proteins that mediate phospholipid transport between organelles at contact sites. Here, we show that the IM-anchored YdbH protein interacts with the OM lipoprotein YnbE to form a functional protein bridge between the IM and OM in *E. coli*. Based on AlphaFold-Multimer predictions, genetic data, and in vivo site-directed cross-linking, we propose that YnbE interacts with YdbH through β-strand augmentation to extend the continuous hydrophobic β-groove of YdbH that is thought to shield acyl chains of phospholipids as they travel through the aqueous intermembrane periplasmic compartment. Our data also suggest that the periplasmic protein YdbL prevents extensive amyloid-like multimerization of YnbE in cells. We, therefore, propose that YdbL has a chaperone-like function that prevents uncontrolled runaway multimerization of YnbE to ensure the proper formation of the YdbH-YnbE intermembrane bridge.

outer membrane biogenesis | AsmA-like proteins | lipid transport | transenvelope complex | membrane contact sites

Didermic bacteria such as *Escherichia coli* and other gram-negative bacteria have a multilayered cell envelope composed of two essential membranes, an aqueous compartment known as the periplasm and a thin peptidoglycan cell wall (1). While the inner membrane (IM), which surrounds the cytoplasm, is a typical phospholipid bilayer, the outer membrane (OM) mostly comprises lipopolysaccharides (LPS) in the outer leaflet and phospholipids in the inner leaflet (2). This asymmetric structure makes the OM a selective permeable barrier against hydrophobic compounds, including many antibiotics and detergents (3, 4). In addition, the OM is stiffer than the IM because of the presence of LPS and its high content of integral OM proteins that adopt a highly stable β-barrel conformation (5). Consequently, the OM protects the cell against rupture caused by internal turgor pressure, and its biogenesis is essential for survival (6, 7).

Components of the OM are produced either in the cytoplasm or at the IM, so they must be transported across the cell envelope and assembled at the OM during growth and division. The biogenesis pathways for LPS (8), OM β-barrel proteins (9, 10), and OM lipoproteins (11, 12) are well known. In contrast, how phospholipids are transported to the OM is poorly characterized. Recently, three members of the AsmA-like protein family, YhdP, TamB, and YdbH, have been shown to maintain OM lipid homeostasis and are proposed to have a redundant role in phospholipid trafficking between IM and OM in *E. coli* (13, 14). Although biochemical evidence of transport is lacking, a growing body of evidence supports their proposed function (13–16). Single-cell microscopy studies unveiled that the loss of YhdP reduces the flow of lipids from the IM to the OM (15). Although the individual loss of YhdP, TamB, or YdbH at most confers minor defects in OM permeability in *E. coli*, their combined loss is lethal, demonstrating that these proteins are redundant in performing a function that is essential for growth (13, 14). Furthermore, phospholipids accumulate in the IM of cells lacking these three AsmA-like paralogs (14). Recent bioinformatics and structural modeling have led to classifying the bacterial AsmA-like proteins as members of the repeating β-groove (RBG) superfamily, which includes eukaryotic lipid-transfer proteins that mediate bulk lipid transport between organelles (16–18). Given these in vivo data and evolutionary connections, and the fact that phospholipid transport

Significance

Bridge-like protein structures are emerging as a conserved mechanism to transport lipids between organelles. These structures connect two membranes to efficiently move multiple lipids per transporter through a continuous hydrophobic groove proposed to shield the acyl chains of lipids as they travel through an aqueous cellular compartment. The bacterial AsmA-like proteins are the ancestors of the repeating β-groove superfamily that includes proteins that bridge organelles in eukaryotic cells to transport lipids. Here, we show that the AsmA-like YdbH protein interacts with the lipoprotein YnbE to form a bridge connecting the inner and outer membranes (OMs) of *Escherichia coli*. We propose that this complex is one of several intermembrane bridges that didermic bacteria possess to translocate lipids to build their OMs.

to the OM is the last known essential process in OM biogenesis to be characterized, the simplest model is that YhdP, TamB, and YdbH transport phospholipids between the IM and OM. In contrast, the function of smaller (<700 amino acids) AsmA-like paralogs (AsmA, YicH, and YhjG) found in many bacteria including *E. coli* remains undetermined as genetic analyses did not find functional connections between them and the larger (>850 amino acids) paralogs YhdP, TamB, and YdbH (13, 16).

It has been proposed that YhdP, TamB, and YdbH form bridge-like structures that resemble that of intermembrane lipid transporters found in eukaryotic cells and didermic bacteria (13–16). These three proteins are predicted to have an N-terminal single transmembrane domain that anchors them to the IM and a long periplasmic region of various lengths formed by repeats of RBG domains (17). The N terminus of this periplasmic region contains a 100- to 150-residue Chorein-N domain that is also found in eukaryotic lipid-transfer proteins like VPS13 and ATG2, which transport lipids between organelles at membrane contact sites (19–22). It has recently been proposed that these eukaryotic lipid transporters and the bacterial AsmA-like proteins form a continuous rod-like structure that is analogous to the periplasmic bridge of the Lpt system, which transports LPS across the periplasm from the IM to the OM (16). The Lpt system forms a multiprotein transenvelope molecular machine that bridges the IM and OM of many didermic bacteria like *E. coli*. The periplasmic Lpt bridge is composed of β-jellyroll domains from different proteins that assemble into a long structure that connects the IM and OM and provides a continuous hydrophobic groove that shields the acyl chains of LPS as this glycolipid travels through the aqueous periplasm (8, 23). Supporting this similarity, the crystal structure of a C-terminal segment (amino acids 963 to 1,138) of the *E. coli* AsmA-like paralog TamB shows a β-taco fold with a hydrophobic groove that resembles the β-jellyroll domains of Lpt proteins (24). Furthermore, AlphaFold2 has predicted that the six *E. coli* AsmA-like proteins and eukaryotic RBG lipid-transfer proteins form bridge-like structures of various lengths and superhelicity that contain a hydrophobic groove (16–18, 25). More recently, a preprint has presented photocross-linking and molecular dynamics data supporting the model that YhdP bridges the IM and OM and transports phospholipids through its hydrophobic groove (26).

If phospholipid transport between the IM and OM occurs through protein bridges, these structures must be ~250 Å to span the width of the periplasm (27). AlphaFold2 predicts that the periplasmic domain of YhdP is long enough to bridge the IM and OM (16), which is further supported by recent negative staining electron microscopy of purified YhdP proteins (26). Even though YhdP and TamB are similar in size (1,259 and 1,266 amino acids, respectively), the AlphaFold2 model for TamB predicts its periplasmic domain is ~160 Å because of higher superhelicity (16). However, TamB is known to physically interact with the Omp85-family OM β-barrel proteins BamA, TamA, and TOC75 in bacteria and chloroplasts (28–30), so TamA/BamA/TOC75-TamB complexes connect the IM and OM. In agreement, we also previously showed that TamA is required for TamB's function in OM biogenesis in *E. coli* (13). In contrast, YdbH is only 869 amino acids, and its periplasmic structure is predicted to only be ~180 Å in length, suggesting that it would need a partner(s) to reach the OM (16).

Here, we present genetic and biochemical evidence that YdbH forms a complex with the OM lipoprotein YnbE. These proteins are encoded in an operon that also encodes the periplasmic protein YdbL. Using genetic analyses, we established that YnbE is required for YdbH's function and that overexpression of *ydbL* causes a negative effect on YdbH/YnbE function. Through in vivo photocross-linking, we found that YnbE forms multimers and interacts with the C terminus of YdbH. Based on our current findings and previous studies

(13–15), we propose a model in which YdbH interacts with the OM lipoprotein YnbE to form a bridge-like structure that participates in phospholipid transport between the IM and OM.

Results

Prediction of YdbH-YnbE-YdbL Complex Formation by AlphaFold-Multimer. AlphaFold2 predicts that YdbH's structure is too short (~180 Å) to span the width (~250 Å) of the periplasm (16, 25, 31), raising the possibility that it might interact with other envelope proteins to bridge the IM and OM. Since *ydbH* is in an operon with *ynbE* and *ydbL*, which are predicted to encode an OM lipoprotein and a periplasmic protein, respectively (Fig. 1 *A* and *B*), we investigated whether YdbH interacts with YnbE and/or YdbL. We first searched for possible interactions using AlphaFold-Multimer since it has successfully predicted protein complexes (32–35). Predicted structures of YdbH, YnbE, and YdbL (*SI Appendix*, Fig. S1 *A–C*) are available in the AlphaFold database (25), but we used their mature amino acid sequences to generate models of YdbH-YnbE-YdbL complexes with a 1:1:1 stoichiometry with AlphaFold-Multimer (32). The model with the highest confidence predicts that the C terminus of YdbH interacts with both YnbE and YdbL (Fig. 1*C* and *SI Appendix*, Fig. S1*D*).
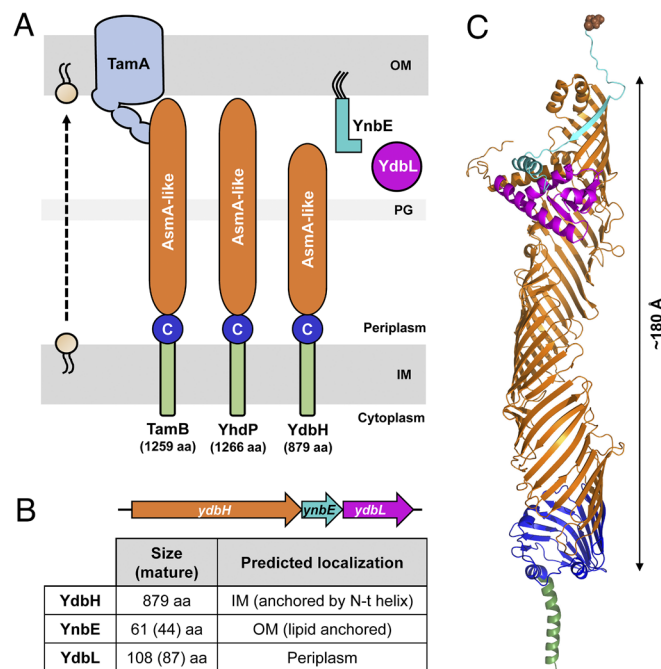

Fig. 1. AlphaFold-Multimer structural prediction of the YdbH-YnbE-YdbL complex. (*A*) TamB, YhdP, and YdbH are members of the AsmA-like protein family and proposed to mediate transport (dotted arrow) of phospholipids across the envelope to build the OM. TamB, YhdP, and YdbH are anchored to the IM by an N-terminal transmembrane helix (green) and have a periplasmic chorein-N domain (C; blue) and an AsmA-like domain (orange) that varies in size. TamA, an OM β-barrel protein, forms a complex with TamB and is necessary for its function in *E. coli* (13, 16, 28, 37). The OM lipoprotein YnbE and the periplasmic protein YdbL are encoded in an operon with *ydbH*. PG refers to peptidoglycan cell wall. (*B*) Structure of the *ydbH-ynbE-ydbL* operon (*Top*). The size and predicted cellular localization of the proteins encoded by this operon are shown (*Bottom*). The size of mature (after signal sequence cleavage) YnbE and YdbL is shown in parenthesis. (*C*) Cartoon representation of the predicted structure of the YdbH-YnbE-YdbL complex by AlphaFold-Multimer. The color scheme used is the same as in panel *A*. The conserved N-terminal cysteine that gets lipidated and anchors YnbE to the OM is shown as brown spheres. The estimated length of the predicted periplasmic structure of YdbH is shown on the *Right*. PyMOL Molecular Graphics System Version 2.5.1 (Schrödinger, LCC) was used to generate images and measure the length of YdbH's periplasmic region.

The predicted interaction between the OM lipoprotein YnbE and the C-terminal domain of YdbH agrees with the expected cellular localization and topology of these proteins (Fig. 1 *A* and *B*). There are no major differences between the model structures of YdbH and YdbL as monomers and in the YdbH-YnbE-YdbL complex; however, while monomeric YnbE is predicted to be largely unstructured except for a small helix at its C terminus (residues K48 to T56), it forms a β-strand between residues I30 and I38 that aligns parallel with the last β-strand of the periplasmic domain of YdbH in the YdbH-YnbE-YdbL complex (Fig. 1*C* and *SI Appendix*, Fig. S1). In this β-strand of YnbE, polar residues (T31, N33, N35, and K37) are predicted to be exposed to the periplasm while nonpolar residues (I30, I32, M34, V36, and I38) would extend the hydrophobic β-groove running along the periplasmic domain of YdbH that is proposed to shield the acyl chains of phospholipids as they transit through the aqueous periplasm. The predicted change in YnbE structure from being disordered as a monomer to folding into a β-strand that associates through parallel β-strand interactions with a partner to extend a β-sheet resembles the behavior of amyloids, raising the possibility that YnbE might multimerize to extend the hydrophobic β-groove even further toward the OM (36). Together, these predictions suggest that YdbH-YnbE-YdbL forms an IM-OM complex in which YnbE extends the hydrophobic β-groove of YdbH.

YdbH and YnbE Function Together. Before testing any of the above structural predictions, we investigated whether YnbE and YdbL are functionally linked to YdbH in *E. coli*. As reported for the Δ*ydbH* mutant (13), we could not detect any growth or OM-permeability defects in the Δ*ynbE* and Δ*ydbL* single mutants. Next, we tested the effect of deleting *ynbE* or *ydbL* in cells lacking TamB and YhdP since the Δ*tamB*, Δ*yhdP*, and Δ*ydbH* alleles are synthetic lethal (13, 14). Growth of a YhdP-depletion strain lacking *tamB* and *ydbH* requires the presence of arabinose in the media to drive the transcription of *yhdP* from the P$_{BAD}$ promoter (P$_{BAD}$::*yhdP*) (13, 14). We therefore constructed and characterized YhdP-depletion strains lacking *tamB* and either *ynbE* or *ydbL*. We found that while the Δ*tamB* Δ*ynbE* P$_{BAD}$::*yhdP* strain, like the Δ*tamB* Δ*ydbH* P$_{BAD}$::*yhdP* strain, requires arabinose to grow, the Δ*tamB* Δ*ydbL* P$_{BAD}$::*yhdP* strain does not (Fig. 2*A*). We also could not detect phenotypic differences between the Δ*tamB* Δ*yhdP* and Δ*tamB* Δ*yhdP* Δ*ydbL* strains. Thus, both YdbH and YnbE, but not YdbL, are essential in cells lacking TamB and YhdP. These data suggest that YdbH and YnbE function together, but we cannot rule out a possible accessory role for YdbL in YdbH/YnbE function.

YdbL Affects the Function of YdbH/YnbE. To further probe functional and protein interactions between YdbH, YnbE, and YdbL, we used a plasmid carrying *ydbH-ynbE-ydbL* that suppresses envelope defects in a Δ*tamB* Δ*yhdP* double mutant (13). Specifically, a Δ*tamB* Δ*yhdP* mutant forms mucoid colonies (because the Rcs envelope stress response is highly activated) and cannot grow on MacConkey agar (because it is sensitive to bile salts owing to its severe OM-permeability defects); the pET23/42YdbH/YnbE/YdbL plasmid suppresses both phenotypes in a Δ*tamB* Δ*yhdP* strain. Therefore, to investigate functional connections between YdbH, YnbE, and YdbL, we monitored whether the mucoid phenotype and MacConkey sensitivity of the Δ*tamB* Δ*yhdP* double mutant could be suppressed by plasmids carrying *ydbH*, *ynbE*, or *ydbL* alone or in different combinations (Fig. 2*B*). We used the pET23/42-based plasmid system in which genes are expressed from an uncharacterized plasmid-encoded promoter that is constitutively active at low levels in the absence of T7 RNA polymerase (38–41). Since the loss of either YdbH or YnbE is lethal in cells lacking TamB
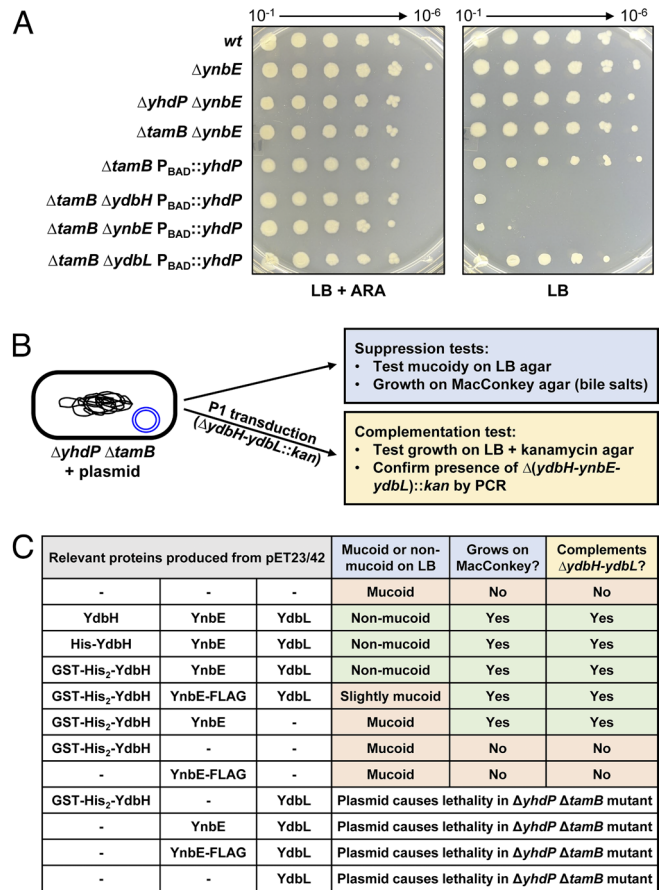

Fig. 2. YdbH and YnbE are essential for growth in a Δ*tamB* Δ*yhdP* mutant. (*A*) The essentiality of *ydbH*, *ynbE*, and *ydbL* in the absence of TamB and YhdP was tested using a Δ*tamB* P$_{BAD}$::*yhdP* strain carrying single Δ*ydbH*, Δ*ynbE*, or Δ*ydbL* chromosomal alleles. Previously, growth of the Δ*tamB* Δ*ydbH* P$_{BAD}$::*yhdP* mutant was shown to be arabinose dependent (13). Overnight cultures grown in LB with arabinose at 37 °C were serially diluted 1:10 in LB and dilutions were stamped with a pin replicator onto LB agar with or without arabinose. Plates were grown at 37 °C for 24 h. (*B*) Strategy to test the function of plasmid-encoded *ydbH*, *ynbE*, and *ydbL* alleles by determining their ability to suppress and complement in the double mutant Δ*tamB* Δ*yhdP* strain NR5161. The Δ*tamB* Δ*yhdP* mutant is mucoid on LB plates, sensitive to bile salts, and unable to grow in the absence of YdbH (13). The presence of a Δ(*ydbH-ynbE-ydbL*)::*kan* chromosomal allele was confirmed by PCR. (*C*) Results from testing suppression and complementation tests as described in panel *B*. Suppression results in nonmucoid colonies on LB and growth on MacConkey agar. Complementation results in viable kanamycin-resistant transductants. Strains used are listed in *SI Appendix*, Table S1. We could not obtain viable NR5161 transformants carrying the pET23/42GST-His₂-YdbH/YdbL, pET23/42YnbE/YdbL, pET23/42YnbE-FLAG/YdbL, and pET23/42YdbL plasmids (see main text for details on this dominant-negative effect). Data are representative of three independent experiments.

Relevant proteins produced from pET23/42			Mucoid or non-mucoid on LB	Grows on MacConkey?	Complements Δ*ydbH*-*ydbL*?
-	-	-	Mucoid	No	No
YdbH	YnbE	YdbL	Non-mucoid	Yes	Yes
His-YdbH	YnbE	YdbL	Non-mucoid	Yes	Yes
GST-His₂-YdbH	YnbE	YdbL	Non-mucoid	Yes	Yes
GST-His₂-YdbH	YnbE-FLAG	YdbL	Slightly mucoid	Yes	Yes
GST-His₂-YdbH	YnbE	-	Mucoid	Yes	Yes
GST-His₂-YdbH	-	-	Mucoid	No	No
-	YnbE-FLAG	-	Mucoid	No	No
GST-His₂-YdbH	-	YdbL	Plasmid causes lethality in Δ*yhdP* Δ*tamB* mutant		
-	YnbE	YdbL	Plasmid causes lethality in Δ*yhdP* Δ*tamB* mutant		
-	YnbE-FLAG	YdbL	Plasmid causes lethality in Δ*yhdP* Δ*tamB* mutant		
-	-	YdbL	Plasmid causes lethality in Δ*yhdP* Δ*tamB* mutant		

and YhdP (Fig. 2*A*), we also performed complementation tests on the various plasmids by checking whether they could support growth of a Δ*tamB* Δ*yhdP* Δ(*ydbH-ynbE-ydbL*) mutant (Fig. 2*B*).

As expected, the plasmid carrying *ydbH-ynbE-ydbL* fully suppressed and complemented in cells lacking TamB and YhdP (Fig. 2*C* and *SI Appendix*, Fig. S2). In addition, since we ultimately wanted to monitor protein levels and probe protein interactions, we constructed plasmids encoding N-terminal (cytoplasmic) tags in YdbH and a C-terminal FLAG tag in YnbE. We found that the tagged YdbH variants are fully functional when produced from plasmids also encoding YnbE and YdbL (Fig. 2*C* and *SI Appendix*, Fig. S2). The *ynbE-flag* allele is nearly fully functional when present in plasmids encoding both YdbH and YdbL since these plasmids complemented, suppressed bile salt sensitivity, and partially suppressed mucoidy in the Δ*tamB* Δ*yhdP* mutant (Fig. 2*C*). This plasmid-based system also confirmed that YdbH and YnbE, but not YdbL, are

essential in cells lacking TamB and YhdP since the presence of both plasmid-encoded *ydbH* and *ynbE* was necessary and sufficient to support the growth of a strain with chromosomal deletions in Δ*tamB*, Δ*yhdP*, and Δ(*ydbH-ynbE-ydbL*) (Fig. 2*C*).

Although YdbL is not required for YdbH/YnbE to support the growth of Δ*tamB* Δ*yhdP* cells, our data suggested that YdbL affects their function. First, a plasmid encoding GST-His₂-YdbH and YnbE (and not YdbL) supported growth of the Δ*tamB* Δ*yhdP* Δ(*ydbH-ynbE-ydbL*) mutant and suppressed the MacConkey sensitivity but did not suppress the mucoid phenotype of the Δ*tamB* Δ*yhdP* mutant (Fig. 2*C*). Second, plasmids encoding only *ydbL*, *ydbH* and *ydbL*, or *ynbE* and *ydbL* surprisingly caused lethality in the Δ*tamB* Δ*yhdP* mutant (Fig. 2*C*), but not in the wild type or the Δ*tamB* or Δ*yhdP* single mutants. Thus, the Δ*tamB* Δ*yhdP* mutant, which still encodes a wild-type chromosomal *ydbH-ynbE-ydbL* locus, is viable when it carries plasmids encoding *ydbH-ynbE-ydbL*, *ydbH-ynbE*, *ydbH*, or *ynbE*, but dies when it carries plasmids encoding *ydbH-ydbL*, *ynbE-ydbL*, or *ydbL* (Fig. 2*C*). These results indicate that higher expression of *ydbL* with respect to *ydbH* and *ynbE* causes a dominant-negative phenotype that results in the death of the Δ*tamB* Δ*yhdP* mutant. Because the viability of the Δ*tamB* Δ*yhdP* mutant requires functional YdbH/YnbE, this lethality suggests that excess YdbL decreases YdbH/YnbE function.

Levels of YdbH Decrease in the Absence of YnbE and/or YdbL. Since our genetic analyses showed that YdbH function requires YnbE and that YdbL levels also influence YdbH/YnbE function, we next investigated whether levels of functional N-terminally tagged YdbH were affected by the loss of YnbE and/or YdbL. Immunoblotting with α-His antibodies revealed that although we could not detect His-YdbH, we could readily detect both GST-His-YdbH and GST-His₂-YdbH in three distinct bands, two of which (the slowest migrating bands) were also visible in α-GST immunoblots (*SI Appendix*, Fig. S3 *A* and *B*). These results suggest that the GST tag facilitates detection of His-tagged YdbH even though GST-His-YdbH and GST-His₂-YdbH likely undergo some partial degradation of GST (i.e., fastest migrating band only visible in α-His blots). Although we do not fully understand why these tagged proteins yield multiple bands, our subsequent analyses showed that the three species behave the same. Since GST-His₂-YdbH demonstrated the best detection and was fully functional, we used it in the experiments described below.

Analysis of whole-cell lysates of Δ(*ydbH-ynbE-ydbL*) cells carrying various plasmids revealed that the levels of YdbH were ~50% reduced in the absence of YnbE, but its migration pattern did not change (*SI Appendix*, Fig. S3*C*). In the absence of YdbL, there was a less pronounced decrease in YdbH levels (*SI Appendix*, Fig. S3*C*). Surprisingly, the presence of a C-terminal FLAG tag in YnbE led to similarly lower levels of YdbH that were not further reduced in the absence of YdbL (*SI Appendix*, Fig. S3*C*). These results, together with the fact that both pET-GST-His₂-YdbH/YnbE and pET-GST-His₂-YdbH/YnbE-FLAG/YdbL cannot fully suppress the mucoid phenotype of the Δ*tamB* Δ*yhdP* mutant (Fig. 2*C*), suggest that either the FLAG-tag in YnbE decreases YdbL function or that the *ynbE-flag* allele reduces translation of *ydbL* by affecting *ynbE-ydbL* translational coupling. Altogether, the fact that YnbE and YdbL are necessary for the proper levels of YdbH agrees with the model for a functional, and possibly physical, connection between these proteins.

YnbE Structure Is Affected by YdbH and YdbL. We next wanted to monitor YnbE and YdbL levels using our plasmid system. Unfortunately, despite multiple attempts to insert tags at various sites, we could not detect YdbL using immunoblotting, so

hereafter we only used plasmids encoding untagged YdbL. In contrast, we could easily detect functional YnbE-FLAG using α-FLAG immunoblotting in samples from wild-type cells carrying pET23/42GST-His₂-YdbH/YnbE-FLAG/YdbL (*SI Appendix*, Fig. S4). YnbE-FLAG migrated as a ~12 kDa band likely corresponding to the monomer as well as several high-molecular-weight (HMW) bands that exhibited increased intensity and slower mobility when the whole-cell lysate was boiled possibly because of amyloid-like multimerization and/or aggregation (*SI Appendix*, Fig. S4*B*). Next, we monitored YnbE-FLAG levels produced from plasmids lacking YdbH and/or YdbL in Δ(*ydbH-ynbE-ydbL*) cells. We found that levels of YnbE-FLAG decreased in the absence of YdbH (*SI Appendix*, Fig. S5). It is possible that this effect is caused by the disruption of the strong translational coupling between the *ydbH-ynbE* gene pair, made possible by their overlapping stop and start codons (ATGA) and intragenic Shine-Dalgarno motifs inside the *ydbH* gene that are important for the termination and reinitiation of translation in the *ydbH-ynbE* gene pair (42). In the absence of YdbL, there was only a modest increase in the intensity of HMW species of YnbE-FLAG (*SI Appendix*, Fig. S5). However, when only YnbE was produced from the plasmid (in the absence of YdbH and YdbL), we observed a further increase in the signal of the HMW species and a decrease in the level of monomeric YnbE-FLAG (*SI Appendix*, Fig. S5). These findings suggest that YdbH and YdbL impact YnbE's structure and ability to multimerize and/or aggregate.

The C-Terminal Domain of YdbH Interacts with YnbE In Vivo. Since our in vivo data revealed a functional relationship between YdbH, YnbE, and YdbL, we next probed whether they interact with each other. We first confirmed using immunoblotting analysis of cell fractionations that, as predicted, YnbE is present in the OM (*SI Appendix*, Fig. S6). YdbH is mainly enriched in the IM, but can also be easily detected in the OM, suggesting that this protein might be part of an intermembrane bridge (*SI Appendix*, Fig. S6). We then tested the validity of the AlphaFold-Multimer predictions of the YdbH-YnbE-YdbL complex using in vivo site-specific photocross-linking. Since we could not detect YdbL and AlphaFold-Multimer predicts that YdbH and YnbE still interact in the absence of YdbL, we focused on probing interactions between the C terminus of YdbH and YnbE (Fig. 3 *A* and *B*).

Site-specific photocross-linking relies on the generation of amber alleles of a gene of interest that can be suppressed by a specialized tRNA that is charged with a UV-cross-linkable unnatural amino acid such as *p*-benzoyl-L-phenylalanine (*p*BPA). Exposure of cells producing the resulting protein variants to UV can lead to the formation of cross-links between the unnatural amino acid and carbon atoms within ~2 Å (43). Cross-linked species can be detected by a mass shift in immunoblots. We performed in vivo photocross-linking experiments in cells producing GST-His₂-YdbH(*p*BPA) variants with *p*BPA substitutions near its C terminus, with a few of them being predicted to interact with YnbE or YdbL by AlphaFold-Multimer. Out of the 12 variants produced from the pET23/42GST-His₂-YdbH(*p*BPA)/YnbE-FLAG/YdbL plasmid, those with *p*BPA substitutions at W791 and W857 demonstrated UV-dependent cross-links in YdbH (Fig. 3 *B* and *C* and *SI Appendix*, Fig. S7). These cross-linked species could not be detected in cells carrying plasmids lacking YnbE but persisted in the absence of YdbL (Fig. 3*D*). Interestingly, AlphaFold-Multimer models predict that YdbH residue W791 is close to YnbE in both YdbH-YnbE-YdbL and YdbH-YnbE complexes, but residue W857 in YdbH is predicted to interact with YnbE only in the YdbH-YnbE model. Together, our results suggest that YnbE and the C-terminal region of YdbH physically interact in cells and that YdbL is not required for this interaction.
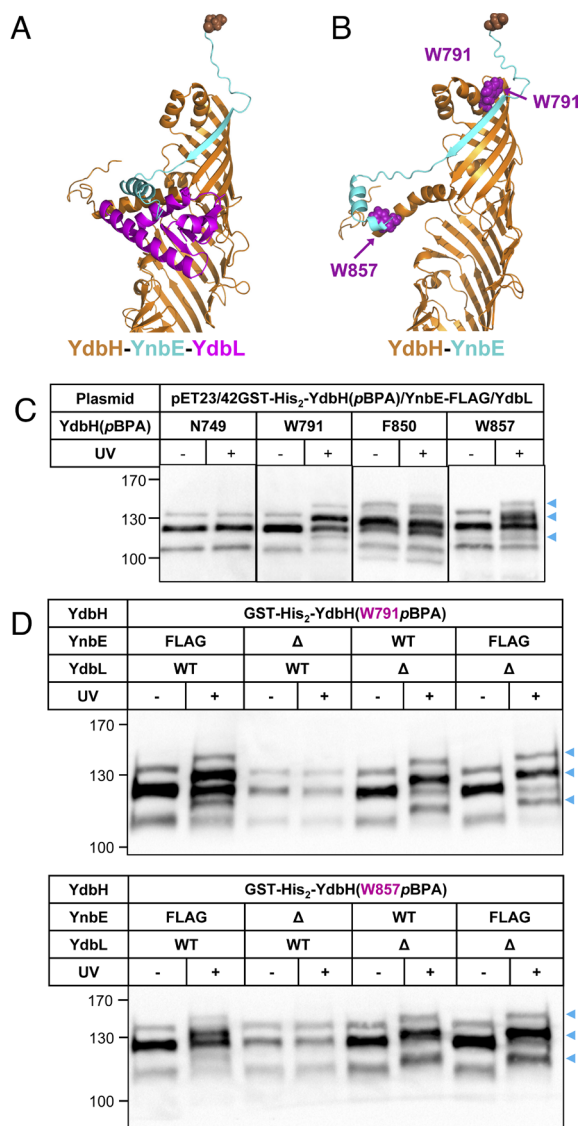
Fig. 3. The C-terminal domain of YdbH interacts with YnbE in vivo. Cartoon representations of AlphaFold-Multimer predictions of the YdbH-YnbE-YdbL (*A*) and YdbH-YnbE (*B*), complexes. Images were generated by PyMOL Molecular Graphics System Version 2.5.1 (Schrödinger, LCC). (*C*) Immunoblots testing for the formation of YdbH(*p*BPA) cross-links. Plasmid-encoded GST-His$_2$-YdbH(*p*BPA) variants were produced in MG1655 Δ(*ydbH-ynbE-ydbL*)::*kan*. Exponentially growing cells were exposed or not to UV light for 30 min. Proteins from nonboiled whole-cell lysate samples were resolved in a 6% (w/v) SDS-polyacrylamide gel and subjected to α-His immunoblotting. Molecular mass markers (in kDa) are shown on the *Left*. (*D*) Immunoblots showing that UV-dependent cross-linked adducts of GST-His$_2$-YdbH(*p*BPA) are dependent on YnbE and independent of YdbL. GST-His$_2$-YdbH(*p*BPA) variants with substitutions at W791 and W857 were produced from plasmids lacking either *ynbE* or *ydbL* in MG1655 Δ(*ydbH-ynbE-ydbL*)::*kan* cells to test for dependence of YdbH cross-links on YnbE and YdbL. Cells and samples were treated as in panel *C*. Blue arrowheads mark bands corresponding to YdbH-YnbE cross-links. Immunoblots are representative of three independent experiments.

YnbE Multimerizes and Interacts with YdbH In Vivo. We further tested the formation of YdbH-YnbE complexes as well as the possibility that YnbE multimerizes as suggested by our immunoblots of whole-cell samples (*SI Appendix*, Figs. S4 and S5) and AlphaFold-Multimer (Fig. 4*A*) by performing in vivo photocross-linking experiments. We generated 11 YnbE(*p*BPA)-FLAG variants (Fig. 4 *B–D*) that were produced from a plasmid also encoding GST-His$_2$-YdbH and YdbL. Whole-cell lysate samples from cells exposed or not to UV were then analyzed using α-FLAG and α-His immunoblots. The α-FLAG blots showed that all 11 YnbE(*p*BPA)-FLAG variants formed UV-dependent

cross-links, leading to laddering of numerous bands that migrated from ~20 kDa to HMW species (Fig. 4*E* and *SI Appendix*, Fig. S8). Blots showed a prominent ~20 kDa band likely corresponding to a dimer of YnbE-FLAG and HMW bands that could be YnbE multimers formed in *E. coli* cells (Fig. 4*A*). Importantly, when the same samples were blotted with α-His antibodies, we detected a UV-dependent shift in GST-His$_2$-YdbH from cells producing 6 of the YnbE(*p*BPA)-FLAG variants with *p*BPA substitutions at positions I21, V23, D47, V50, E52, and L53, which flank the β-strand that AlphaFold-Multimer predicted to interact with the C-terminal β-strand of YdbH's β-groove (Fig. 4 *E* and *F*). These bands resemble YdbH cross-links observed in Fig. 3 *C* and *D*. These data strongly suggest that YnbE multimerizes and interacts with YdbH in cells.

To test the dependence of YnbE(*p*BPA)-FLAG cross-links on YdbH and YdbL, we carried out photocross-linking experiments on a representative group of 6 YnbE(*p*BPA)-FLAG variants (with *p*BPA substitutions at I21, V23, K27, K37, D47, and E52) produced from plasmids lacking YdbH and a representative group of 5 YnbE(*p*BPA)-FLAG variants (with *p*BPA substitutions at T31, K37, E41, D47, and E52) produced from plasmids lacking YdbL. These YnbE(*p*BPA)-FLAG variants still formed HMW cross-links in the absence of YdbH or YdbL, albeit there were some changes in the laddering pattern of the HMW species (Fig. 4*F* and *SI Appendix*, Fig. S8*B*). As expected, all bands detected in α-His immunoblots disappeared in the absence of GST-His$_2$-YdbH (Fig. 3*G*); however, they were still detected in the absence of YdbL (*SI Appendix*, Fig. S8*B*), indicating that YdbH and YnbE can interact in the absence of YdbL, as predicted by AlphaFold-Multimer (Fig. 3*B*). Importantly, the fact that the ~20 kDa band was still present in the absence of YdbL rules out the idea that this band corresponds to YnbE-YdbL cross-links, suggesting they are likely YnbE dimers. Finally, we also performed cross-linking on the YnbE/K37*p*BPA-FLAG variant produced from plasmids lacking YdbH and/or YdbL and observed an increase in the signal of HMW species upon cross-linking when YdbL was absent (*SI Appendix*, Fig. S9). Together, these data show that YdbH and YnbE form a complex in *E. coli* cells even in the absence of YdbL. In addition, YnbE multimerizes (or aggregates) into HMW species, and formation of these HMW species does not require but is affected by the absence of YdbH and YdbL.

Structural Prediction–Guided Disruption of YdbH-YnbE Function and Complex Formation. To assess the impact of the predicted β-strands of YnbE on its function and interaction with YdbH, we introduced double-proline substitutions to disrupt the secondary structure of YnbE by creating kinks in its predicted β-strand. This approach has been successfully used to investigate the importance of the N- and C-terminal β-strands of EspP and BamA in the assembly of EspP at the OM (44). We hypothesized that the introduction of kinks in YnbE's predicted β-strand would disrupt its alignment with YdbH, diminishing its capacity to effectively interact with YdbH, as well as its ability to multimerize. It is worth noting that the β-strand of YnbE is predicted to be longer in YnbE-YnbE models (residues I30-I44 in one YnbE and residues I32-A46 in the other YnbE) than in YnbE-YdbH models (residues I30-I38). We generated four double-proline variants (N33P/N35P, M34P/V36P, K37P/E39P, H40P/I42P) covering the predicted β-strand of YnbE. Three of these YnbE-FLAG variants (N33P/N35P, M34P/V36P, H40P/I42P) failed to both suppress the MacConkey sensitivity and complement the loss of chromosomal *ydbH-ynbE-ydbL* in the Δ*tamB* Δ*yhdP* mutant (Fig. 5 *A* and *B*). Intriguingly, the YnbE(K37P/E39P)-FLAG variant caused lethality in the Δ*yhdP* Δ*tamB* mutant (Fig. 5 *A* and *B*), indicating that
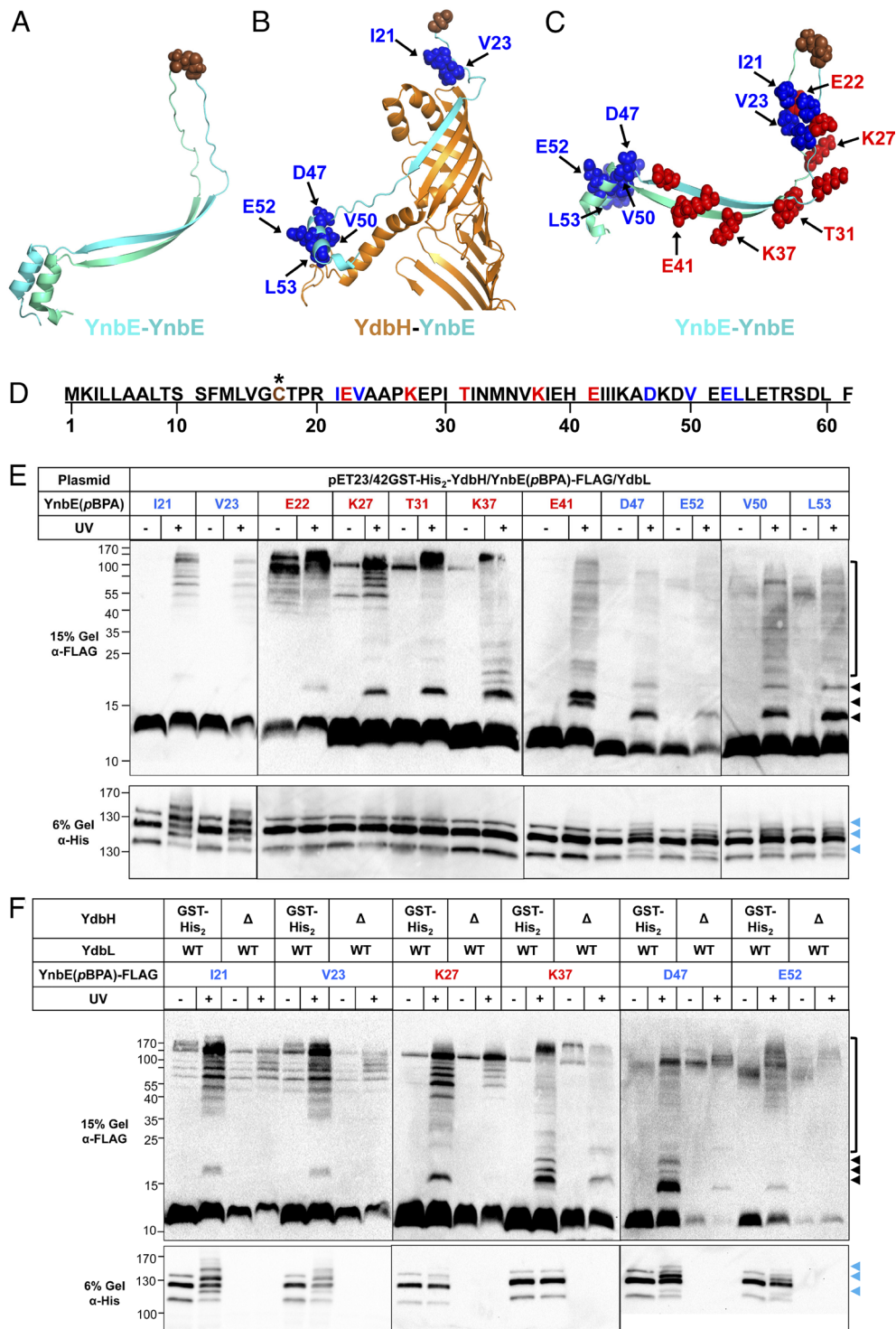
Fig. 4. YnbE multimerizes and interacts with YdbH in vivo. Cartoon representations of AlphaFold-Multimer predictions of the YnbE-YnbE (*A*), YdbH-YnbE (*B*), and YnbE-YnbE (*C*) complexes. Residues substituted with *p*BPA are shown as spheres. Images were generated by PyMOL Molecular Graphics System Version 2.5.1 (Schrödinger, LCC). (*C*) Residues substituted with *p*BPA are shown as spheres in the YnbE-YnbE structural models predicted by AlphaFold-Multimer and colored as in panels *D–F*. (*D*) Amino acid sequence of YnbE. The conserved lipidated cysteine is shown in brown and marked with an asterisk. Amino acids that were substituted with *p*BPA are colored red if they only yielded UV-dependent high-molecular weight adducts or blue if they also yielded UV-dependent YdbH-YnbE cross-links. (*E*) Immunoblots showing cross-linked YnbE(*p*BPA)-FLAG adducts. Exponentially growing wild-type MG1655 producing plasmid-encoded YnbE(*p*BPA)-FLAG variants with *p*BPA substitutions at E22, K27, T31, E41, D47, or E52, or MG1655 Δ(*ydbH-ynbE-ydbL*)::*kan* producing plasmid-encoded YnbE(*p*BPA)-FLAG variants with substitutions at I21, V23, V50, or L53 were exposed (or not) to UV light for 30 min. Proteins from nonboiled whole-cell lysate samples were resolved in 15% and 6% (w/v) SDS-polyacrylamide gels and subjected to α-FLAG and α-His immunoblotting, respectively. Molecular mass markers (in kDa) are shown on the *Left*. All YnbE(*p*BPA)-FLAG variants form HMW cross-links (α-FLAG blots), while those with substitutions at I21, V23, D47, V50, E52, and L53 also caused a UV-dependent shift in GST-His$_2$-YdbH (α-His blots). (*F*) Immunoblots show that HMW YnbE cross-links still form in cells lacking YdbH (α-FLAG blot), while all bands detected in the α-His blot are dependent on the presence of GST-His$_2$-YdbH. Cells carrying a chromosomal Δ(*ydbH-ynbE-ydbL*)::*kan* deletion and producing different plasmid-encoded YnbE(*p*BPA)-FLAG variants from pET23/42GST-His$_2$-YdbH/YnbE(*p*BPA)-FLAG/YdbL or pET23/42YnbE(*p*BPA)-FLAG/YdbL were processed as in panel. Black arrowheads and brackets mark bands corresponding to YnbE-YnbE cross-links, while blue arrowheads mark bands corresponding to YdbH-YnbE cross-links. Immunoblots are representative of three independent experiments.
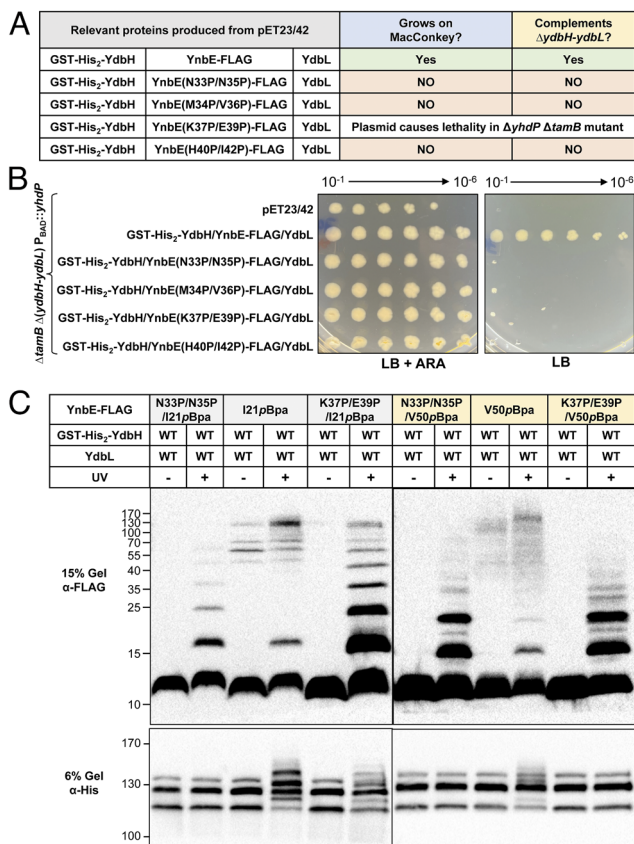
Fig. 5. Predicted β-strand of YnbE is important for function and interaction with YdbH. (*A*) Results from testing suppression and complementation tests for YnbE double-proline variants using methodology described in Fig. 2*B*. (*B*) Plasmid-encoded YnbE-FLAG double-proline variants were tested by their ability to complement (i.e., support the growth of) a Δ*tamB* Δ(*ydbH-ynbE-ydbL*) P_{BAD}::*yhdP* strain in the absence of arabinose. Plasmid-carrying derivatives of the arabinose-dependent Δ*tamB* Δ(*ydbH-ynbE-ydbL*) YhdP-depletion strain were grown overnight in LB with arabinose and ampicillin at 37 °C. Overnight cultures were serially diluted 1:10 in LB and dilutions were stamped with a pin replicator onto LB agar with or without arabinose. Agar plates were grown overnight at 37 °C for 24 h. (*C*) Immunoblots to test the effect of the double-proline N33P/N35P and K37P/E39P substitutions on the ability of YnbE(I21*p*BPA)-FLAG and YnbE(V50*p*BPA)-FLAG to cross-link to GST-His_2-YdbH. Exponentially growing Δ(*ydbH-ynbE-ydbL*)::*kan* cells producing different plasmid-encoded YnbE(*p*BPA)-FLAG variants were exposed (or not) to UV light for 30 min. Proteins from nonboiled whole-cell lysate samples were resolved in 15% and 6% (w/v) SDS-polyacrylamide gels and subjected to α-FLAG and α-His immunoblotting, respectively. Molecular mass markers (in kDa) are shown on the *Left*. Black arrowheads and brackets mark bands corresponding to YnbE-YnbE cross-links, while blue arrowheads mark bands corresponding to YdbH-YnbE cross-links. All data are representative of three independent experiments.

it exhibits a dominant-negative behavior by somehow interfering with the function of chromosomally encoded wild-type YnbE. Immunoblots revealed that for all double proline variants, the levels of monomeric YnbE were comparable to those of wild-type YnbE in Δ*ydbH-ydbL* cells; however, we could not detect the HMW species in samples from the proline variants (*SI Appendix*, Fig. S10). These results show that introducing kinks in its predicted β-strand, renders YnbE nonfunctional and defective in its ability to multimerize. However, they do not provide an explanation for the dominant-negative nature of the K37P/E39P variant.

To directly assess the ability of the double-proline YnbE variants to interact with YdbH and multimerize, we introduced a single *p*BPA substitution (I21*p*BPA or V50*p*BPA) into two double-proline variants (N33P/N35P and K37P/E39P) that are representative of the different phenotypes described above (Fig. 5*A*). As described earlier, YnbE-FLAG variants with either I21*p*BPA or V50*p*BPA showed

UV-dependent cross-links with YdbH and multimerization (Figs. 4*E* and 5*C*). The presence of N33P/N35P or K37P/E39P did not abolish HMW cross-links, but the laddering band pattern of cross-links was inverted (Fig. 5*C*). Specifically, while in samples from the I21*p*BPA or V50*p*BPA, the signal of the laddering bands was most intense in the area corresponding to HMW species, there was an increase in the intensity of bands of lower molecular mass and a decrease in those of higher mass in samples from the proline mutants. The altered pattern suggests that the proline mutants can still multimerize to some extent, but their ability to form stable multimers is compromised. When the same samples were probed for GST-His_2-YdbH, we found that the two *p*BPA variants with the N33P/N35P substitutions failed to show UV-dependent cross-linking to YdbH (Fig. 5*C*). Interestingly, the K37P/E39P substitutions, which cause a dominant-negative effect, also abolished cross-linking of YnbE(V50*p*BPA)-FLAG to YdbH, but only partially reduced the efficiency of YnbE(I21*p*BPA)-FLAG to cross-link to YdbH (Fig. 5*C*). Altogether, we conclude that the alterations we introduced into the predicted β-strand secondary structure of YnbE render the protein nonfunctional. The double-proline substitutions cause defects in YnbE multimerization and its interactions with YdbH. Furthermore, our cross-linking data provide a likely explanation for the dominant-negative behavior of YnbE(K37P/E39P)-FLAG. We propose that this variant exerts dominant-negative effects because it can still interact with YdbH but in an altered way that leads to a defective YdbH-YnbE complex. Since this variant is produced from a plasmid, it must titrate enough YdbH away from chromosomally encoded wild-type YnbE to cause lethality of the Δ*yhdP* Δ*tamB* mutant. In contrast, the other proline variants are not dominant because they do not interact with YdbH.

Discussion

Bulk lipid transport between eukaryotic membrane-bound organelles is mediated by RBG proteins like VPS13 and ATG2 at membrane contact sites (17, 18, 22, 45). These RBG proteins form bridge-like structures that connect to membrane proteins in different organelles and provide a continuous hydrophobic groove that is thought to shield the acyl chains of lipids as they travel through the aqueous interorganelle cytosol (17, 46). It is well established that didermic bacteria such as *E. coli* transport newly synthesized LPS from the IM to the OM through similar bridge-like proteinaceous structures (8, 23, 47). More recently, the bacterial AsmA-like proteins have been identified as ancestors of the eukaryotic RBG lipid-transfer proteins (17) and are proposed to function in transporting phospholipids between the IM and OM of didermic bacteria (13–16). Here we demonstrate that YdbH, an AsmA-like or RBG protein in *E. coli*, forms a transenvelope bridge-like structure by interacting with the OM lipoprotein YnbE. Our data show that YdbH and YnbE are functional partners required for the survival of *E. coli* mutants that lack the functionally redundant AsmA-like proteins TamB and YhdP. We also demonstrate that the periplasmic protein YdbL affects the function and structure of the YdbH-YnbE complex.

Recent studies have shed light on the functional redundancy of YhdP, TamB, and YdbH in maintaining lipid homeostasis at the OM in *E. coli* (13–15). According to the current model, TamB, YhdP, and YdbH form bridge-like structures that facilitate the bidirectional diffusional movement of phospholipids between the IM and OM (13, 14, 16). Experimental evidence supports that TamB is part of an IM-OM complex since it is anchored to the IM, interacts with the OM β-barrel protein TamA, and its function depends on TamA (13, 37, 48). Recent structural predictions and MD simulations have also led to the proposal that YhdP is long enough and

sufficient to bridge the IM and OM (26). However, YdbH is significantly smaller than TamB and YhdP, and its periplasmic domain is predicted to be too short to reach the OM (16). By combining genetic analyses, AlphaFold-Multimer structural predictions, and in vivo photocross-linking, we have shown that YdbH directly interacts with the OM lipoprotein YnbE and that this interaction is required for function. AlphaFold predicts that YdbH folds into an elongated structure composed of short curved β-strands that provide a continuous hydrophobic groove that extends from the IM toward the OM. We propose that YnbE associates through β-strand augmentation with the C-terminal end of YdbH to extend the continuous β-groove of YdbH that facilitates phospholipid transport through the periplasm. Indeed, disrupting the β-strand of YnbE with prolines either prevents or alters its interaction with YdbH and leads to a total loss of YdbH/YnbE function. In wild-type cells, the YdbH-YnbE complex would be stably anchored to the IM via the N-terminal α-helix of YdbH and to the OM via the N-terminal lipid anchor of the YnbE lipoprotein (Fig. 6A).

Our data also showed that YnbE can multimerize. We presume that this polymerization is the result of β-strand augmentation based on AlphaFold-Multimer predictions and the fact that introducing prolines into the β-strand of YnbE dramatically reduces its multimerization. However, it remains to be determined whether the YdbH-YnbE complex includes a single YnbE monomer or a multimer of undefined composition (Fig. 6A). The AlphaFold-Multimer model structure of the complex containing only one YnbE protein is expected to still be too short (~180 Å) to span the width (~250 Å) of the periplasm, but it is possible that the predicted helicity of the RBG domain is wrong so that the periplasmic domain could be longer. Therefore, additional investigations on the composition and structure of the YdbH-YnbE complex are needed.

The *ydbH* and *ynbE* genes are organized into an operon with *ydbL*, which encodes a periplasmic protein. Our data demonstrate that even though YdbL is not required for YdbH/YnbE function,
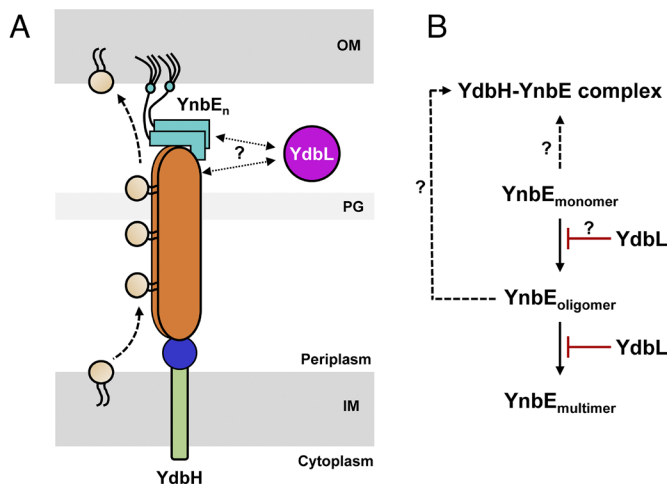
it affects their structure and function. Without YdbL, the levels of YdbH decrease but those of YnbE multimers increase. The loss of YdbH also increases YnbE multimerization, albeit to a lesser level. YnbE multimerization further increases if both YdbH and YdbL are missing. Notably, YdbL is also needed for complete suppression of envelope defects observed in a mutant lacking both YhdP and TamB when *ydbH* and *ynbE* are present in multicopy. Together, these results suggest that YdbL helps (but is not required) in the formation of the YdbH-YnbE complex. Yet, increasing YdbL production is lethal in a *yhdP tamB* double mutant, which relies on YdbH/YnbE function to grow. Thus, YdbL paradoxically exerts a mild positive effect on YdbH/YnbE function when it is produced from the *ydbH-ynbE-ydbL* operon, but it causes a strong negative effect when its production is increased with respect to that of *ydbH* and *ynbE*. Collectively, these pieces of evidence strongly suggest that a proper ratio of YdbL to YdbH/YnbE must be present in cells to maintain YdbH-YnbE function. Below, we propose a model that explains our findings on YdbL.

We propose that YnbE can multimerize and/or interact with the C terminus of YdbH through β-strand augmentation. Although the association between YdbH and YnbE is required for their function in OM lipid homeostasis (presumably transport of phospholipids between the IM and OM), it is unclear, as stated above, how many YnbE proteins form a functional YdbH/YnbE transenvelope complex. However, the fact that the loss of YdbH and YdbL increases multimerization and that YnbE might exhibit amyloid-like behavior raise the possibility that the functional form of YnbE is either monomeric YnbE or an oligomer containing a low number of YnbE proteins and that uncontrolled multimerization of YnbE leads to nonfunctional structures. We therefore propose that YdbL functions to prevent the formation of nonfunctional YnbE multimers (Fig. 6B). In the absence of YdbL, the production of high-order nonfunctional multimers would increase; although enough YnbE would still interact with YdbL (as a monomer or oligomer) to support growth of the *yhdP tamB* double mutant, the nonfunctional multimers would titrate the amount of YnbE that can associate with YdbH, which would likely lead to degradation of free YdbH proteins. This proposal would explain why the loss of YdbL decreases the levels of YdbH while increasing YnbE multimerization. It would also explain why YdbL is not essential for YdbH/YnbE function or complex formation but is required for full multicopy suppression of defects in the *yhdP tamB* mutant. This suppression requires higher amount of YdbH/YnbE complexes than those produced from the native chromosomal locus. This proposed chaperone-like function of YdbL could also explain the strong dominant-negative effect of YdbL overproduction that kills *yhdP tamB* cells. The proposed chaperone-like function of YdbL implies a direct interaction between YnbE and YdbL. If YdbL levels increased with respect to those of YnbE, it could titrate YnbE, preventing its association with YdbH. This titration would be lethal in *yhdP tamB* cells since they need functional YdbH-YnbE complexes to grow. The proposed chaperone function for YdbL resembles that of the periplasmic CsgC chaperone that prevents premature runaway polymerization of the amyloid CsgA protein in the periplasm before its secretion to the environment to produce curli at the cell surface (49).

Fig. 6. Model of the architecture, function, and biogenesis of the YdbH-YnbE complex. (*A*) YdbH forms a bridge between the IM and OM via interactions with a YnbE monomer or oligomer (YnbE$_n$) of unknown composition. This bridge-like structure likely transports multiple phospholipids by shielding their acyl chains as they cross the aqueous periplasm. How the YdbH-YnbE$_n$ complex extracts and delivers phospholipids and direction of transport remain uncharacterized. Whether YdbL interacts with the YdbH-YnbE$_n$ complex is unknown. (*B*) Proposed biogenesis of the YdbH-YnbE complex and chaperone-like function of YdbL. Monomeric YnbE either oligomerizes or directly interacts with YdbH to form a functional YdbH-YnbE complex. Whether this complex contains a YnbE monomer or oligomer is unknown. YnbE can also undergo amyloid-like runaway multimerization into a nonfunctional high-order multimeric state. We propose that YdbL interacts with YnbE to prevent its uncontrolled multimerization and thereby facilitate the proper formation of the YdbH-YnbE complex.

Materials and Methods

Bacterial Strains and Growth Conditions. Strains used in this study are derived from wild-type strain MG1655 (50) and are listed in *SI Appendix*, Table S1. Generalized P1$_{vir}$ transduction was used to move deletion alleles from the Keio collection (51) to the desired strains by selecting for kanamycin resistance. If required, the kanamycin-resistance cassette was excised using Flp recombinase (52). Unless otherwise specified, cells were cultured in lysogeny broth (LB Lennox;

Fisher Scientific) at 37 °C with aeration, and growth was measured using absorbance at 600 nm (OD$_{600}$). Cells were also grown on LB agar containing 15 g/L agar (BD Difco) or MacConkey agar (BD; catalog no. BD281810). When needed, ampicillin (25 or 125 µg/mL), L-arabinose (0.2%, wt/vol), chloramphenicol (20 µg/mL), kanamycin (25 µg/mL), or tetracycline (25 µg/mL) was added to the growth media. For UV photo cross-linking experiments, glucose M63 minimal medium (53) was supplemented with p-benzoyl phenylalanine (pBPA, 0.48 mM) and antibiotics.

Construction of YhdP-Depletion Strain. We previously constructed a YhdP-depletion strain carrying the $yhdP$ (1:: bla araC-P$_{BAD}$) allele (13). Here, we replaced the bla gene (conferring ampicillin resistance) with a kanamycin cassette through recombineering to render the YhdP-depletion strain compatible with our plasmid system (pET23/42; ampicillin resistance). For recombineering, the kanamycin cassette from pKD4 (54) was amplified using the primers blaP1 and blaP1 (*SI Appendix*, Table S2). The PCR product was digested with DpnI (New England Biolabs) and electroporated into recombineering strain DY378 (55) carrying bla-araC-P$_{BAD}$ on the chromosome. Kanamycin-resistant recombinants were selected on LB agar containing kanamycin at 30 °C and validated through PCR. P1$_{vir}$ transduction was used to transfer the $yhdP$ Ω(−1:: kan araC-P$_{BAD}$) allele into other strains by selecting for kanamycin-resistant transductants. YhdP depletion and efficiency of plating protocols were followed as previously described (13).

Site-Directed Mutagenesis (SDM). Primers used in this study are listed in *SI Appendix*, Table S2. SDM PCR was performed using Phusion High-Fidelity DNA Polymerase (Thermo Fischer Scientific) following the manufacturer's protocol. SDM PCR products were digested with DpnI and electroporated into DH5α. Transformants carrying plasmids were selected on LB agar with 125 µg/mL ampicillin. For deletion and insertion SDM, DpnI digested PCR products were treated with T4 polynucleotide kinase (New England Biolabs) and ligated with T4 DNA ligase (New England Biolabs). Plasmid construction was confirmed by DNA Sanger sequencing.

Plasmid Construction. The pET23/42YdbH/YnbE/YdbL (renamed here as pET23/42GST-His-YdbH/YnbE/YdbL) plasmid (13), which encodes a GST-HIS epitope tag upstream of and in-frame with $ydbH$, was modified to improve detection of YdbH by immunoblotting by inserting an additional His$_6$ tag after the start codon of $ydbH$ to produce pET23/42GST-His$_2$-YdbH/YnbE/YdbL. To construct a plasmid producing tag-less YdbH, the region between the NdeI and BamHI sites was deleted using primers listed in *SI Appendix*, Table S2. For immunodetection of YnbE, the sequence encoding a FLAG tag preceded by the linker sequence GSGS was inserted before the stop codon of $ynbE$ to make pET23/42GST-His$_2$-YdbH/YnbE-FLAG/YdbL. The $ydbL$ gene was deleted from pET23/42GST-His$_2$-YdbH/YnbE-FLAG/YdbL generating a "four-base stop signal" sequence (UGAC) which has a low termination efficiency (56). To avoid this potential problem, the TGACTC sequence was replaced with TAATAA (stop codons underlined) to generate pET23/42GST-His$_2$-YdbH/YnbE-FLAGStop. Other insertions and deletions were generated using primer sets listed in *SI Appendix*, Tables S2 and S3 using SDM.

Suppression and Complementation Tests of Mutant Alleles. Plasmid-encoded $ydbH$, $ynbE$, and $ydbL$ mutant alleles were introduced and examined for their ability to suppress the mucoidy (on LB agar) and inability to grow on McConkey agar phenotypes of a Δ$tamB$ Δ$yhdP$ strain (NR5161). Two different approaches were used to test for complementation by the plasmid-encoded mutant alleles. First, we used generalized P1$_{vir}$ transduction to transfer the Δ($ydbH$-$ydbL$)::kan deletion into the chromosomal $ydbH$-$ydbL$ locus of a Δ$tamB$ Δ$yhdP$ strain carrying plasmid-derived mutant alleles. Because $ydbH$ and $ynbE$ are essential in the Δ$tamB$ Δ$yhdP$ strain, transductants were only obtained when the strain carried functional plasmid-borne $ydbH$ and $ynbE$ alleles. Transductants were confirmed by colony PCR. Second, we assessed complementation of plasmid-derived mutant alleles using YhdP-depletion strains [NR7606 = Δ$tamB$ Δ($ydbH$-$ydbL$) P$_{BAD}$::$yhdP$; or NR7813 = Δ$tamB$ Δ$ynbE$ P$_{BAD}$::$yhdP$] and determining their ability to grow on LB agar in the presence or absence of arabinose.

Immunoblot Analysis. Whole cell lysates were prepared from exponentially growing cells (OD$_{600}$ ~ 0.8). To normalize samples by cell density, a volume (in µL) from each culture was taken corresponding to 800 divided by the OD$_{600}$ value of the culture. These culture samples were centrifuged at 16,873 x g for 1 min at room temperature and the resulting cell pellets were resuspended in 50 µL of 1× Laemmli sample buffer and 12.5 units of Benzonase (Novagen), achieving a final

concentration of cells equivalent to OD$_{600}$ ~ 16. These suspensions were either boiled for 10 min or not (for unboiled samples). Equal volumes of samples were loaded onto 6% or 15% SDS-polyacrylamide gels for electrophoresis. Utilizing a semidry transfer cell (Bio-Rad), proteins in gels were transferred to polyvinylidene difluoride (PVDF) membranes at 10 V for 2 h. Membranes were blocked in TBST milk [1X Tris-buffered saline (pH 7.6), 0.1% Tween-20 with 5% (w/v) nonfat dry milk] for 30 min at room temperature. Next, membranes were probed with anti-His (1:10,000; Millipore Sigma), anti-GST (1:1,000; Invitrogen), or anti-FLAG M2 (1:10,000; Millipore Sigma) followed by anti-mouse horseradish peroxidase (1:10,000; GE Healthcare). Clarity Max Western ECL substrate (Bio-Rad) was used to generate the signal, which was detected by a ChemiDoc XRS+ system (Bio-Rad).

Construction and In Vivo Photocross-Linking of Strains. We employed a previously described technique for in vivo photocross-linking experiments (43). Briefly, to build plasmid-encoded $ydbH$ and $ynbE$ amber alleles, sequences encoding specific amino acids were changed to amber stop codons (5'-TAG) using SDM. These plasmids were introduced into strains NR2766 and NR7359 (*SI Appendix*, Table S1), which carry pSUP-BpaRS-6TRN (57). Overnight cultures of the resulting cross-linking strains were diluted into 6 mL of glucose M63 minimal medium supplemented with 20 µg/mL chloramphenicol, 125 µg/mL ampicillin, and 0.48 mM pBPA. When cultures reached OD$_{600}$ ~ 0.8 to 1.0, they were split in half. One half of the culture was left untreated, while the other half was subjected to UV light (365 nm; Spectroline E series) in a 24-well flat-bottom cell culture plate (Costar; Corning Inc.) for 30 min at room temperature. After treatment, cells were pelleted by centrifugation at 16,873 × g for 1 min at room temperature and resuspended in 100 µL of 1× Laemmli sample buffer and 12.5 units of Benzonase (Novagen). Samples were either boiled for 10 min or left unboiled and equal volumes of treated and untreated samples were loaded onto 6% or 15% SDS-polyacrylamide gels for electrophoresis followed by immunoblotting as described above.

AlphaFold Structural Predictions. The AlphaFold Protein Structure Database (25) was leveraged to acquire the model structures for YdbH (UniProt P52645), YnbE (UniProt P64448), and YdbL (UniProt P76076) using the https://alphafold.ebi.ac.uk website. With the support of the Unity server at the Ohio State University, AlphaFold-Multimer (5) was used employing the full-length protein sequence of YdbH and mature sequences (without signal sequence) of YnbE and YdbL as input with default settings to generate five relaxed models of the YdbH-YnbE-YdbL, YdbH-YnbE, and YnbE-YnbE complexes. The best-scored model was used for analysis and presented in a cartoon representation using PyMOL Molecular Graphics System Version 2.5.1 (Schrödinger, LCC).

Separation of IM and OM Fractions. We used a previously described method for IM and OM separation protocol with few modifications (58). Cells were grown in 50 mL of LB with ampicillin to OD$_{600}$ ~ 0.7 to 0.9 and then pelleted by centrifugation at 2,862 × g for 10 min. The cell pellet was washed once with 5 mL of cold 10 mM Tris-HCl (pH 8.0) and then resuspended in 6 mL 10 mM Tris HCl (pH 8.0) and 20% sucrose (wt/wt) containing 1 mM PMSF (phenyl methane sulfonyl fluoride) and 50 µg/mL DNase. Cells were lysed with a One-shot cell disrupter (Constant system) at 8,000 psi. Cell debris and nonlysed cells were pelleted by centrifugation at 2,862 × g for 10 min. Cell lysates were stored at −20 °C until further use. One mL of lysate was layered on top of a two-step sucrose gradient consisting of 40% (1 mL) sucrose solution (wt/wt) in 10 mM Tris HCl (pH 8.0) layered on top of 65% (300 µL) sucrose solution. The IM and OM fractions were separated by ultracentrifugation at 85,024 × g for 16 h (Beckman Coulter, model: Optima Max-TL Ultra; TLS-55 Rotor). Fractions of 80 µL were then collected from the top of the tube and analyzed using immunoblotting. To identify the IM and OM fractions, LptD antiserum (1:10,000 dilution) that can cross-react with an unidentified 55 kDa IM protein and the OM protein OmpA was used (38). Additionally, as an OM marker, LPS was probed with a mouse anti-LPS (1:10,000 dilution; Bio-Rad).

Data, Materials, and Software Availability. All study data are included in the article and/or *SI Appendix*.

1. T. J. Silhavy, D. Kahne, S. Walker, The bacterial cell envelope. *Cold Spring Harb. Perspect. Biol.* **2**, a000414 (2010).
2. Y. Kamio, H. Nikaido, Outer membrane of Salmonella typhimurium: Accessibility of phospholipid head groups to phospholipase c and cyanogen bromide activated dextran in the external medium. *Biochemistry* **15**, 2561–2570 (1976).
3. H. Nikaido, Molecular basis of bacterial outer membrane permeability revisited. *Microbiol. Mol. Biol. Rev.* **67**, 593–656 (2003).
4. J. C. Henderson *et al.*, The power of asymmetry: Architecture and assembly of the gram-negative outer membrane lipid bilayer. *Annu. Rev. Microbiol.* **70**, 255–278 (2016).
5. I. V. Mikheyeva, J. Sun, K. C. Huang, T. J. Silhavy, Mechanism of outer membrane destabilization by global reduction of protein content. *Nat. Commun.* **14**, 5715 (2023).
6. E. R. Rojas *et al.*, The outer membrane is an essential load-bearing element in Gram-negative bacteria. *Nature* **559**, 617–621 (2018).
7. J. Berry, M. Rajaure, T. Pang, R. Young, The spanin complex is essential for lambda lysis. *J. Bacteriol.* **194**, 5667–5674 (2012).
8. E. Lundstedt, D. Kahne, N. Ruiz, Assembly and maintenance of lipids at the bacterial outer membrane. *Chem. Rev.* **121**, 5098–5123 (2021).
9. D. Tomasek, D. Kahne, The assembly of beta-barrel outer membrane proteins. *Curr. Opin. Microbiol.* **60**, 16–23 (2021).
10. M. T. Doyle, H. D. Bernstein, Function of the Omp85 superfamily of outer membrane protein assembly factors and polypeptide transporters. *Annu. Rev. Microbiol.* **76**, 259–279 (2022).
11. J. El Rayes, R. Rodriguez-Alonso, J. F. Collet, Lipoproteins in Gram-negative bacteria: New insights into their biogenesis, subcellular targeting and functional roles. *Curr. Opin. Microbiol.* **61**, 25–34 (2021).
12. M. Grabowicz, Lipoproteins and their trafficking to the outer membrane. *EcoSal Plus* **8**, 1–8 (2019).
13. N. Ruiz, R. M. Davis, S. Kumar, YhdP, TamB, and YdbH are redundant but essential for growth and lipid homeostasis of the gram-negative outer membrane. *mBio* **12**, e0271421 (2021).
14. M. V. Douglass, A. B. McLean, M. S. Trent, Absence of YhdP, TamB, and YdbH leads to defects in glycerophospholipid transport and cell morphology in Gram-negative bacteria. *PLoS Genet.* **18**, e1010096 (2022).
15. J. Grimm *et al.*, The inner membrane protein YhdP modulates the rate of anterograde phospholipid flow in Escherichia coli. *Proc. Natl. Acad. Sci. U.S.A.* **117**, 26907–26914 (2020).
16. S. Kumar, N. Ruiz, Bacterial AsmA-like proteins: Bridging the gap in intermembrane phospholipid transport. *Contact (Thousand Oaks)* **6**, 25152564231185931 (2023).
17. S. D. Neuman, T. P. Levine, A. Bashirullah, A novel superfamily of bridge-like lipid transfer proteins. *Trends Cell Biol.* **32**, 962–974 (2022).
18. M. Hanna, A. Guillen-Samander, P. De Camilli, RBG motif bridge-like lipid transport proteins: Structure, functions, and open questions. *Annu. Rev. Cell Dev. Biol.* **39**, 409–434 (2023), 10.1146/annurev-cellbio-120420-014634.
19. B. Ugur, W. Hancock-Cerutti, M. Leonzino, P. De Camilli, Role of VPS13, a protein with similarity to ATG2, in physiology and disease. *Curr. Opin. Genet. Dev.* **65**, 61–68 (2020).
20. M. Leonzino, K. M. Reinisch, P. De Camilli, Insights into VPS13 properties and function reveal a new mechanism of eukaryotic lipid transport. *Biochim. Biophys. Acta Mol. Cell Biol. Lipids* **1866**, 159003 (2021).
21. D. G. McEwan, K. M. Ryan, ATG2 and VPS13 proteins: Molecular highways transporting lipids to drive membrane expansion and organelle biogenesis. *FEBS J.* **289**, 7113–7127 (2022).
22. S. K. Dziurdzik, E. Conibear, The Vps13 family of lipid transporters and its role at membrane contact sites. *Int. J. Mol. Sci.* **22**, 2905 (2021).
23. D. J. Sherman *et al.*, Lipopolysaccharide is transported to the cell surface by a membrane-to-membrane protein bridge. *Science* **359**, 798–801 (2018).
24. I. Josts *et al.*, The structure of a conserved domain of TamB reveals a hydrophobic beta taco fold. *Structure* **25**, 1898–1906.e5 (2017).
25. J. Jumper *et al.*, Highly accurate protein structure prediction with AlphaFold. *Nature* **596**, 583–589 (2021).
26. B. F. Cooper *et al.*, Phospholipid transport to the bacterial outer membrane through an envelope-spanning bridge. bioRxiv [Preprint] (2023). https://doi.org/10.1101/2023.10.05.561070 (Accessed 6 October 2023).
27. V. R. Matias, A. Al-Amoudi, J. Dubochet, T. J. Beveridge, Cryo-transmission electron microscopy of frozen-hydrated sections of Escherichia coli and Pseudomonas aeruginosa. *J. Bacteriol.* **185**, 6112–6118 (2003).
28. C. J. Stubenrauch, T. Lithgow, The TAM: A translocation and assembly module of the beta-barrel assembly machinery in bacterial outer membranes. *EcoSal Plus* **8**, 103–111 (2019).
29. H. Iqbal, M. R. Kenedy, M. Lybecker, D. R. Akins, The TamB ortholog of Borrelia burgdorferi interacts with the beta-barrel assembly machine (BAM) complex protein BamA. *Mol. Microbiol.* **102**, 757–774 (2016).
30. Y. L. Chen *et al.*, TIC236 links the outer and inner membrane translocons of the chloroplast. *Nature* **564**, 125–129 (2018).
31. A. T. Asmar *et al.*, Communication across the bacterial cell envelope depends on the size of the periplasm. *PLoS Biol.* **15**, e2004303 (2017).
32. R. Evans *et al.*, Protein complex prediction with AlphaFold-multimer. bioRxiv [Preprint] (2022). https://doi.org/10.1101/2021.10.04.463034 (Accessed 7 July 2022).
33. M. R. MacRae *et al.*, Protein-protein interactions in the Mla lipid transport system probed by computational structure prediction and deep mutational scanning. *J. Biol. Chem.* **299**, 104744 (2023).
34. J. S. Park, J. Hu, N. M. Hollingsworth, G. Miltenberger-Miltenyi, A. M. Neiman, Interaction between VPS13A and the XK scramblase is important for VPS13A function in humans. *J. Cell Sci.* **135**, jcs260227 (2022).
35. A. Guillen-Samander *et al.*, A partnership between the lipid scramblase XK and the lipid transfer protein VPS13A at the plasma membrane. *Proc. Natl. Acad. Sci. U.S.A.* **119**, e2205425119 (2022).
36. P. Charoenkwan *et al.*, AMYPred-FRL is a novel approach for accurate prediction of amyloid proteins by using feature representation learning. *Sci. Rep.* **12**, 7697 (2022).
37. J. Selkrig *et al.*, Discovery of an archetypal protein transport system in bacterial outer membranes. *Nat. Struct. Mol. Biol.* **19**, 506–510, S1 (2012).
38. T. Wu *et al.*, Identification of a protein complex that assembles lipopolysaccharide in the outer membrane of Escherichia coli. *Proc. Natl. Acad. Sci. U.S.A.* **103**, 11754–11759 (2006).
39. S. Kumar, F. A. Rubino, A. G. Mendoza, N. Ruiz, The bacterial lipid II flippase MurJ functions by an alternating-access mechanism. *J. Biol. Chem.* **294**, 981–990 (2019).
40. F. A. Rubino *et al.*, Detection of transport intermediates in the peptidoglycan flippase MurJ identifies residues essential for conformational cycling. *J. Am. Chem. Soc.* **142**, 5482–5486 (2020).
41. S. Kumar, N. Ruiz, Probing conformational states of a target protein in Escherichia coli cells by in vivo cysteine cross-linking coupled with proteolytic gel analysis. *Bio. Protoc.* **9**, e3271 (2019).
42. M. Huber *et al.*, Translational coupling via termination-reinitiation in archaea and bacteria. *Nat. Commun.* **10**, 4006 (2019).
43. J. W. Chin, A. B. Martin, D. S. King, L. Wang, P. G. Schultz, Addition of a photocrosslinking amino acid to the genetic code of Escherichiacoli. *Proc. Natl. Acad. Sci. U.S.A.* **99**, 11020–11024 (2002).
44. C. Shen *et al.*, Structural basis of BAM-mediated outer membrane beta-barrel protein assembly. *Nature* **617**, 185–193 (2023).
45. J. A. Lees, K. M. Reinisch, Inter-organelle lipid transfer: A channel model for Vps13 and chorein-N motif proteins. *Curr. Opin. Cell Biol.* **65**, 66–71 (2020).
46. A. Ghanbarpour, D. P. Valverde, T. J. Melia, K. M. Reinisch, A model for a partnership of lipid transfer proteins and scramblases in membrane expansion and organelle biogenesis. *Proc. Natl. Acad. Sci. U.S.A.* **118**, e2101562118 (2021).
47. T. W. Owens *et al.*, Structural basis of unidirectional export of lipopolysaccharide to the cell surface. *Nature* **567**, 550–553 (2019).
48. J. Selkrig *et al.*, Conserved features in TamA enable interaction with TamB to drive the activity of the translocation and assembly module. *Sci. Rep.* **5**, 12905 (2015).
49. M. L. Evans *et al.*, The bacterial curli system possesses a potent and selective inhibitor of amyloid formation. *Mol. Cell* **57**, 445–455 (2015).
50. F. R. Blattner *et al.*, The complete genome sequence of Escherichia coli K-12. *Science* **277**, 1453–1462 (1997).
51. T. Baba *et al.*, Construction of Escherichia coli K-12 in-frame, single-gene knockout mutants: The Keio collection. *Mol. Syst. Biol.* **2**, 2006.0008 (2006).
52. P. P. Cherepanov, W. Wackernagel, Gene disruption in Escherichia coli: TcR and KmR cassettes with the option of Flp-catalyzed excision of the antibiotic-resistance determinant. *Gene* **158**, 9–14 (1995).
53. K. Elbing, R. Brent, Media preparation and bacteriological tools. *Curr. Protoc. Mol. Biol.* **Chapter 1**, Unit 1 1 (2002).
54. K. A. Datsenko, B. L. Wanner, One-step inactivation of chromosomal genes in Escherichia coli K-12 using PCR products. *Proc. Natl. Acad. Sci. U.S.A.* **97**, 6640–6645 (2000).
55. D. Yu *et al.*, An efficient recombination system for chromosome engineering in Escherichia coli. *Proc. Natl. Acad. Sci. U.S.A.* **97**, 5978–5983 (2000).
56. E. S. Poole, C. M. Brown, W. P. Tate, The identity of the base following the stop codon determines the efficiency of in vivo translational termination in Escherichia coli. *EMBO J.* **14**, 151–158 (1995).
57. Y. Ryu, P. G. Schultz, Efficient incorporation of unnatural amino acids into proteins in Escherichia coli. *Nat. Methods* **3**, 263–265 (2006).
58. M. V. Douglass, F. Cleon, M. S. Trent, Cardiolipin aids in lipopolysaccharide transport to the gram-negative outer membrane. *Proc. Natl. Acad. Sci. U.S.A.* **118**, e2018329118 (2021).